

First-principles study of lattice dynamics and diffusion in DO₃-type Fe₃Si

S. Dennler* and J. Hafner

Institut für Materialphysik and Center for Computational Materials Science, Universität Wien, Sensengasse 8, A-1090 Wien, Austria

(Received 7 February 2006; published 17 May 2006)

The collective and single-particle dynamics in the intermetallic compound Fe₃Si with the DO₃ structure have been investigated using first-principles density-functional calculations in combination with statistical mechanics in the grand-canonical ensemble. The dispersion relations and the density of states of phonons have been calculated using a direct force-constant approach based on analytic Hellmann-Feynman forces. The defect formation parameters $\Delta\epsilon_D$ and ΔV_D describing the change in energy and volume on removing an atom from the system (D=vacancy) or on substituting an atom by another atomic species (D=antistructure defect) have been determined by total-energy calculations on large supercells. With this information, the grand-canonical potential is calculated as a function of the defect concentrations. Minimization of this potential with respect to the defect concentrations, together with the Gibbs-Duhem relation and the condition of particle-number conservation at fixed composition, determines the effective defect formation enthalpies and volumes. Defect migration enthalpies have been derived from transition states determined using the nudged-elastic-band method. All calculations are based on large 128-atom supercells, as required by the long-range nature of interatomic forces in intermetallic compounds. Phonon dispersion relations and defect formation enthalpies are in good agreement with the available experimental data. The analysis of the defect formation and migration enthalpies explains the pronounced asymmetry between Fe and Si diffusion characteristic of Fe₃Si and leads to a convincing atomistic scenario for the diffusion events.

DOI: 10.1103/PhysRevB.73.174303

PACS number(s): 66.30.Fq, 63.20.Dj, 61.72.Bb, 71.15.Nc

I. INTRODUCTION

The interest in iron-rich intermetallic compounds is based on a wide range of potential applications including high-temperature structural materials, functional materials for magnetic applications, diffusion barriers, contacts, and interconnections in microelectronics.¹ Fe aluminides and Fe silicides are considered for structural applications because they unite high strength with excellent corrosion resistance in oxidizing and sulfiding environments.^{2,3} The Fe-rich compounds Fe₃Al and Fe₃Si possess a very high magnetic susceptibility which makes them useful as soft magnetic materials. Fe₃Si/Fe-Si multilayers have been investigated in relation to possible applications in the field of giant magnetoresistance.^{4,5} Very recently, there has been a strong interest in Fe₃Si films epitaxially grown on semiconducting substrates (Si, GaAs) due to their potential application in magnetoelectronic and spintronic devices—e.g., for spin injection into semiconductors.^{6–8}

Both Fe₃Al and Fe₃Si crystallize over a wide composition range in the DO₃ structure (BiF₃-type, Pearson symbol cF16).^{9–11} Fe₃Al is formed on cooling by ordering reactions from a disordered body-centred cubic solid solution (A2 phase), first into a phase with the B2 (CsCl-type) structure and then below 550 °C into the DO₃ structure illustrated in Fig. 1. Fe atoms occupy the α and γ sublattices, Al atoms the β sublattice. Stoichiometric Fe₃Si exhibits DO₃ order up to its incongruent melting point at 1220 °C. The phase field of DO₃-type Fe_{1-x}Si_x alloys extends over the composition range $0.15 < x < 0.25$. Alloys with $x < 0.23$ undergo a DO₃-B2 transformation at elevated temperatures; the transition temperature decreases from about 1200 °C for the nearly stoichiometric alloys to 800 °C at $x=0.15$. The remarkable difference in the transition temperatures for the order-disorder

transition indicates a much stronger bonding between unlike atoms in Fe₃Si than in Fe₃Al. Both compounds order ferromagnetically at low temperatures; the Curie temperature decreases with decreasing Fe content, reaching a value of $T_c \sim 450$ K at the stoichiometric composition.^{9–11}

The formation of the ordered DO₃ phases and their physical properties at elevated temperatures depend very crucially on the formation of thermal vacancies and their mobility.^{12–16} For this reason vacancy formation^{17,18} and in particular diffusion^{19–33} in the DO₃-type compounds Fe₃Si, Fe₃Al, and Ni₃Sb have been studied extensively using different experimental techniques. In an attempt to explain the outstanding diffusion behavior of these materials in terms of a “phonon-enhanced diffusion” suggested by Petry *et al.*³⁴ for the bcc metals, phonon dispersion relations have been measured for Fe₃Si (Refs. 35 and 36), Fe₃Al (Ref. 37), and Ni₃Sb (Ref. 38). The results of the experimental studies of diffusion demonstrate a rather exceptional scenario for diffusion in DO₃-type Fe₃Si: (i) Fe diffusion is a very fast process in the intermetallic compounds with the DO₃ structure; Fe self-

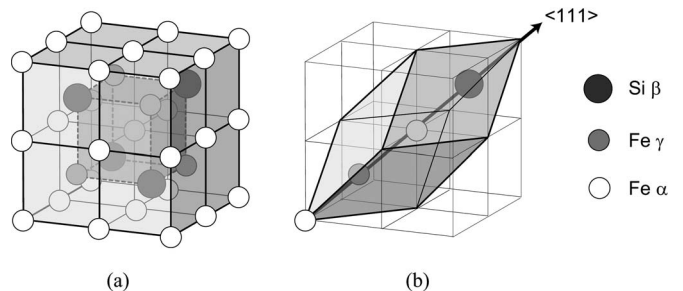


FIG. 1. The DO₃ structure: (a) 16-atom cubic cell, (b) 4-atom primitive cell.

diffusion increases strongly in the sequence α -Fe-Fe₃Al-Fe₃Si. Thermal vacancy concentrations increase in the same sequence, as demonstrated by positron annihilation^{17,39} and differential dilatometry experiments.⁴⁰ (ii) In Fe₃Si the diffusion of the majority component (Fe) is orders of magnitude faster than that of the minority component (Si). This stands in marked contrast to Fe₃Al where the diffusion rates of both components are comparable. (iii) Fe diffusion in Fe₃Si is strongly composition dependent; diffusion is fastest in the nearly stoichiometric alloy. (iv) The diffusion asymmetry in Fe₃Si is considerably reduced above the DO₃-B2 transition temperature, whereas Fe diffusion in Fe₃Al is only slightly affected by the DO₃-B2-A2 transitions. (v) There is a remarkable difference between Fe diffusion in DO₃-type Fe₃Si and in FeSi with the B20 structure: Fe diffusion is very fast in Fe₃Si and very slow in FeSi. (vi) No correlation between the fast diffusion and soft phonon modes could be detected,^{35,36} ruling out “phonon enhancement” as the driving mechanism of the fast diffusion. Migration enthalpies estimated from the phonon densities of states (according to a model proposed by Schober *et al.*⁴¹) are higher at each composition in the Fe-Si system than in the Fe-Al system. As the activation enthalpy for diffusion is the sum of the vacancy formation enthalpy and the migration enthalpy, the much faster diffusion of Fe in Fe₃Si than in Fe₃Al can be understood only in terms of a much lower vacancy formation enthalpy.

The straightforward interpretation of these results is that fast Fe diffusion occurs via nearest-neighbor jumps mediated by thermal vacancies which are present in high concentrations on the Fe sublattice. However, little is known about the diffusion of Si atoms. Given the DO₃ structure, the slow Si diffusion could be explained either by postulating that only order-conserving jumps within the Si sublattice (i.e., over larger than nearest-neighbor distances) occur or by diffusion via antisite defects requiring a rather high formation energy.

A notable attempt to determine the effective formation energies of vacancies and antistructure atoms in Fe₃Si was made by Fähnle and Schimmele⁴² using *ab initio* density-functional calculations in combination with statistical mechanics, following earlier work on DO₃-type Fe₃Al and Ni₃Sb by the same group,^{43,44} and a similar investigation of B2-FeAl (Ref. 45), and B2-NiAl (Ref. 46). The calculations have been performed on supercells of rather modest size, but in combination, these results still shed a very interesting light on the order-disorder transitions and the diffusion properties of the DO₃-type compounds: (i) In Ni₃Sb, the enthalpies of formation for vacancies on the metal sublattices (α and γ) and for Ni-antisite defects on the β sublattice are very low (0.2 to 0.4 eV), but one order of magnitude higher for vacancies on Sb sites and for Sb-antisite atoms on α and γ sites. (ii) For Fe₃Al, vacancy formation enthalpies are 1.25, 2.27, and 1.39 eV on the α , γ and β sublattices. Fe-antisite atoms on the β sublattice and Al-antisite defects on the γ sublattice have almost zero formation enthalpies, whereas Al-antisite atoms on the α site require a high formation enthalpy of 1.82 eV. (iii) In Fe₃Si vacancy formation enthalpies are 1.14 and 1.52 eV on the Fe sublattice and 2.82 eV on the Si sublattice, respectively. The formation of antisite-defects requires a modest formation energy of 0.45 eV on the

Fe sublattices, but a large enthalpy of 2.85 eV on the Si sublattice. These results rationalize many of the experimental observations: (i) The dominant structural defects in these compounds are Ni vacancies in Ni₃Sb, but antisite defects in both Fe₃Al and Fe₃Si. (ii) The vacancy concentration is higher on the α than on the γ sublattice and very low in Ni₃Sb and Fe₃Si (but not in Fe₃Al). For both Fe₃Si and Fe₃Al these results contradict the assumptions made in the interpretation of quasielastic²¹ and static⁴⁷ Mössbauer experiments, postulating the absence of γ vacancies in Fe₃Si (Ref. 21) and the presence of γ vacancies in Fe₃Al (Ref. 47). The interpretation of the diffusion data requires the further assumption that the activation energies for diffusion are dominated by the defect formation energies, while there are only smaller differences in the migration energies for the various jump processes. While the difference in the vacancy formation enthalpies is certainly large enough to explain the drastically reduced diffusivity of the minority component in Ni₃Sb and in Fe₃Si, it is much more difficult to decide on the relative importance of $\alpha \rightarrow \beta$ and $\alpha \rightarrow \gamma$ nearest-neighbor jumps and of correlated diffusion events—this definitely requires an analysis of the migration enthalpies as well.

This is precisely the aim of the present work, where we report first-principles investigations of the collective and single-particle dynamics in Fe₃Si. We have performed a detailed calculation of the phonon spectrum and of the defect formation and migration enthalpies using advanced density-functional methods. Due to the rather long-range nature of the interatomic forces in intermetallic compounds, this is a rather demanding task. The calculations of phonons, defects, and diffusion energies have been performed on large 128-atom supercells. Our paper is organized as follows: In Sec. II we describe our computational method and we review results on the structural, cohesive, electronic, and magnetic properties of Fe₃Si in comparison to previous calculations and experiments. Section III presents our results on the phonon dispersion relations and density of states and an estimate of the average migration energy derived from the vibrational spectrum. Section IV summarizes our results on the defect formation enthalpies; activation energies for various atomistic diffusion processes are given in Sec. V. Our conclusions are presented in Sec. VI.

II. COMPUTATIONAL DETAILS

Our calculations were carried out within the density functional framework (DFT) using the Vienna *ab initio* simulation package^{48,49} (VASP) implementing the projector-augmented wave (PAW) method.^{50,51} The plane-wave basis set contained components with energies up to 300 eV while the Brillouin zone was sampled using Monkhorst-Pack meshes of \mathbf{k} points⁵² adapted to the size of the computational cell as detailed below. The geometric relaxation was performed with a quasi-Newton algorithm using the exact Hellmann-Feynman forces, with a criterion for stopping the structural optimization of 0.05 eV/Å. To speed up convergence, we employed a Methfessel-Paxton smearing with a width of 0.1 eV. Magnetism was fully taken into account through a spin-polarized DFT approach. The spin interpola-

tion formula of Vosko, Wilk, and Nusair, which is known to give reasonable results, was used.⁵³ Local magnetic moments were calculated by integrating the magnetization densities within atom-centered spheres with radii of 1.302 and 1.312 Å for Fe and Si, respectively. All these parameters were carefully checked to give reasonably accurate results.

The influence of nonlocal corrections in the exchange-correlation functional has been already largely investigated in the literature. In particular, an earlier extensive study⁵⁴ by Moroni *et al.* using the same DFT code (but using ultrasoft pseudopotentials instead of PAW's) has demonstrated that the use of the generalized gradient approximation (GGA) is mandatory to describe correctly the stability of the bulk phases, the lattice parameters, the cohesive energies, and the magnetic properties of Fe-Si compounds. Here, the GGA functional proposed by Perdew, Burke, and Ernzerhof⁵⁵ (PBE) was employed. Using a sufficiently dense Monkhorst-Pack grid of $12 \times 12 \times 12$ for the primitive cubic cell of bulk DO_3 Fe_3Si , the obtained lattice constant $a=2.802$ Å agrees very well with the experimental value¹¹ $a=2.825$ Å and is similar to the value determined by Moroni *et al.* with the GGA functional of Perdew and Wang⁵⁶ (PW91), $a_W=2.815$ Å. On the other hand, a too small lattice constant of 2.745 Å is found within the local density approximation (LDA). The magnetic moments obtained within the GGA, $\mu_{\text{Fe}_\alpha}=1.33\mu_B$, $\mu_{\text{Fe}_\gamma}=2.56\mu_B$, and $\mu_{\text{Si}_\beta}=-0.11\mu_B$, are also in good agreement with experimental estimations⁵⁷ $\mu_{\text{Fe}_\alpha}=1.35\mu_B$, $\mu_{\text{Fe}_\gamma}=2.2\mu_B-2.4\mu_B$, and $\mu_{\text{Si}_\beta}=-0.07\mu_B$. The different values of the magnetic moments on the Fe sites correlate with the local coordination: Fe atoms on γ sites with a larger magnetic moment have eight Fe nearest neighbors (NN) and six Si as next-nearest neighbors (NNN). Fe atoms on α sites with a lower magnetic moment have a NN shell with four Fe and four Si atoms. Hence the formation of a high magnetic moment (which is even slightly increased relative to pure Fe) is correlated to a high number of Fe neighbors. The nonmagnetic solution is less stable by 0.26 eV/atom and exhibits a smaller lattice constant of 2.775 Å. For the magnetic properties we note again a good agreement with the results of Moroni *et al.*⁵⁴ and with the linear-muffin-tin-orbital calculation of Kulikov *et al.*⁵⁸ and Kudrnovsky *et al.*⁵⁹ Kulikov *et al.* also showed that the large magnetic energy of the DO_3 phase is essential for stabilizing the ordered DO_3 phase relative to the disordered $B2$ phase. In the following, the results fully take magnetism into account.

The relaxed defect structures have been determined via a conjugate-gradient algorithm,⁶⁰ using analytic Hellmann-Feynman forces on the atoms and stresses on the supercell. Equilibrium is reached if the force on the atoms becomes less than 0.05 eV/Å in each of the Cartesian directions. Diffusion barriers are determined using the nudged-elastic-band (NEB) method.^{61,62} In the NEB method a reaction coordinate relating initial and final states is defined and a set of intermediate states (images) is distributed along the reaction path. The “images” are coupled by elastic forces to ensure continuity of the reaction path. Each intermediate state is fully relaxed in the hyperspace perpendicular to the reaction coordinate. The specific computational setup that we used to compute the phonon dispersion curves and the effective de-

fect formation energies are discussed in the following corresponding sections.

III. PHONON SPECTRUM

The phonon dispersion relation of DO_3 Fe_3Si alloy was calculated using a direct *ab initio* approach.⁶³ In this method, the force constant matrix is derived in the harmonic approximation from the exact forces calculated via the Hellmann-Feynman theorem in a reduced set of total-energy calculations where each of the inequivalent atoms is successively displaced along each direction. Then the phonon dispersion curve can be computed through the diagonalization of the dynamical matrix for arbitrary \mathbf{k} vector. Note that for \mathbf{k} vectors compatible with the periodic boundary conditions applied to the supercell, the phonon frequencies calculated via this direct *ab initio* approach are identical with the results of an exact frozen-phonon calculation. Compared to other methods based on the linear response,⁶⁴ the advantage of this technique is that only a very small set of static calculations is sufficient to determine the dynamical matrix for arbitrary \mathbf{k} , whereas the response calculation has to be repeated for every new wave vector.

Due to the long range of the interaction, the force-constant approach requires very large supercells. Our phonon calculations are based on *ab initio* calculations using a large 128-atom cubic supercell constructed by repeating the cell of Fig. 1(a) twice in the three directions. The resulting supercell has a side of about 11.2 Å. A fine Monkhorst-Pack grid of $4 \times 4 \times 4$ was employed to ensure high-precision total-energy calculations. These parameters were checked to lead to well-converged phonon dispersion curves.

As illustrated in Fig. 2, the obtained phonon frequencies are in very good agreement with earlier results from inelastic neutron scattering experiments³⁵ at 20 °C. The accuracy of the *ab initio* calculations is comparable to that of a 16-parameter Born-von Karman fit used to analyze the experimental data—this confirms the accuracy of the calculated Hellmann-Feynman forces and lends credibility to the calculation of the defect formation and migration enthalpies. A particular motivation of the experimental investigation of phonon dispersion relations was to check whether the fast diffusion in Fe_3Si could eventually be explained by a “phonon-enhanced” diffusion mechanism. The lowest phonon branches are the transverse acoustic (TA) branches, reaching frequencies of about 4 THz at the Brillouin-zone boundary. These frequencies are comparable to those of the TA branches in crystalline Si. The dispersion relations of the TA branches are essentially monotonous, except for a certain flattening on approaching the X point, again similar as in Si. The TA frequencies are relatively modest, indicating low-potential-energy barriers for nearest-neighbor jumps, but there is no indication for soft phonons eventually causing a phonon enhancement of the diffusion rates like in the bcc high-temperature phases of transition metals.

In a second step, the phonon density of states $Z(\nu)$ was determined from the dispersion curves shown in Fig. 2 by integration over the Brillouin zone, using a fine $30 \times 30 \times 30$ grid. The result, shown in Fig. 2, shows that the phonon

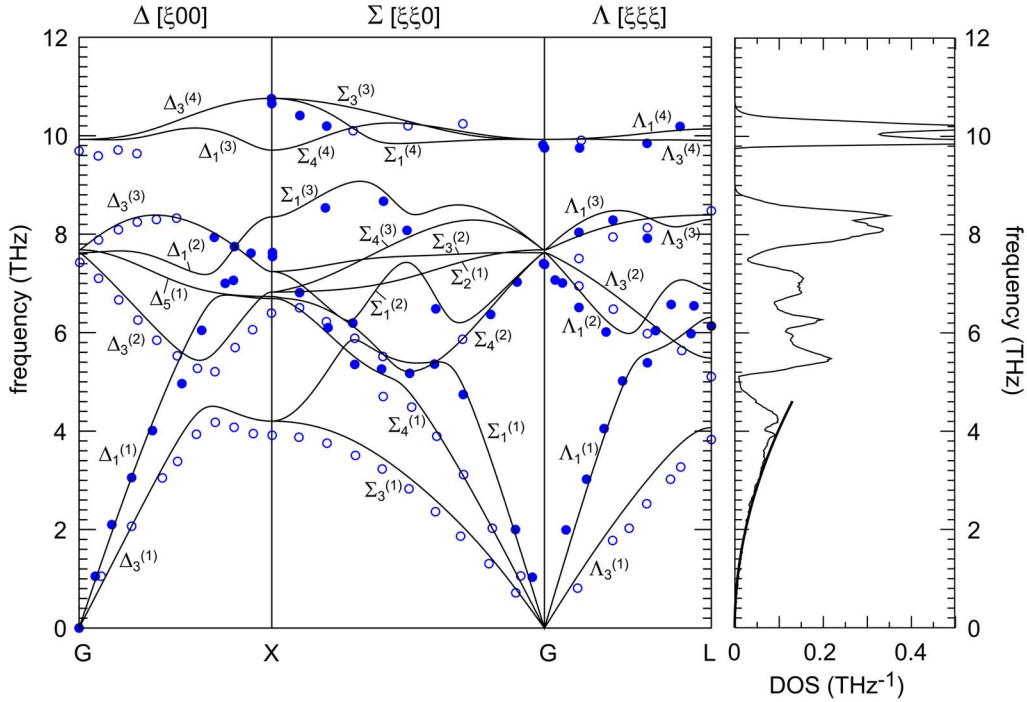


FIG. 2. (Color online) Phonon dispersion and phonon density of states (DOS) in $\text{DO}_3 \text{Fe}_3\text{Si}$ alloy as obtained from our *ab initio* calculations (solid lines) and from inelastic neutron scattering experiments (Ref. 35) at 20 °C (dots). The fit in the DOS shows its ν^2 dependence at low frequency.

DOS has only a small weight at low frequencies. Compared to the DOS derived from the Born–van Karman fit to the inelastic neutron data, our *ab initio* calculations show a slightly less pronounced peak at the zone-boundary frequencies of the lowest acoustic modes, but the Debye temperature we determined from the ν^2 dependence of $Z(\nu)$ at low frequency, $\nu_D=377$ K, remains of the same order as the value stemming from the experiments, $\nu_D^{\text{expt}}=444$ K.

The elastic constants C_{11} , C_{12} , and C_{44} can be derived from the slopes of the phonon acoustic branches.⁶⁵ For a cubic structure we have seven equations to determine the three independent elastic constants. We have checked that the calculated elastic constants (Table I) are self-consistent, the differences never exceeding 0.01 Mbar. For comparison we have also calculated the elastic constants from the linear

stress-strain relations, using the least-squares extraction method proposed by Le Page and Saxe (Ref. 66; see also Jahnátek *et al.*⁶⁷). The accuracy of our calculations may be further checked by comparing the bulk modulus $B_{\text{phon}}=2.18$ Mbar derived from the slope of the dispersion relations of the acoustic phonons or from the stress-strain relation $B_{\text{stress}}=2.24$ Mbar with that derived from a homogeneous deformation (i.e., the second derivative of the total energy as a function of volume), $B_{\text{def}}=2.20$ Mbar. Table I compares our results with the available experimental data. The comparison with experiment is not easy, since there are significant differences between the different sets of experimental values, in particular for the bulk modulus. The values reported by Kötter *et al.* have been used by Randl *et al.* in the Born–von Karman fit to the inelastic neutron data. Even

TABLE I. Experimental and calculated elastic constants C and bulk modulus B of the $\text{Fe}_3\text{Si DO}_3$ crystal (in Mbar). B , C' , and C_L are calculated according $B=(C_{11}+2C_{12})/3$, $C'=(C_{11}-C_{12})/2$, and $C_L=(C_{11}+C_{12}+2C_{44})/2$.

Results	C_{11}	C_{12}	C_{44}	B	C'	C_L
From phonons ^a	3.08	1.73	1.32	2.18	0.68	3.73
From stress/strain ^a	3.00	1.87	1.48	2.24	0.57	3.92
Kötter <i>et al.</i> ^b	2.19	1.43	1.37	1.68	0.38	3.18
Rausch <i>et al.</i> ^c	2.43	1.59	1.40	1.87	0.42	3.41
Drickamer <i>et al.</i> ^d				2.50		

^aPresent work.

^bReference 68.

^cReference 69.

^dReference 70.

if the agreement between theory and experiment might appear to be quite modest from a first look at the tabulated elastic constants, the comparison of the full set of acoustic dispersion relations shows that the agreement is still quite reasonable.

From the phonon density of states (DOS) $Z(\nu)$ the migration enthalpy H_M can be estimated according the method proposed by Schober *et al.*:⁴¹

$$H_M^{phon} = 4\pi^2 a^2 \alpha \left(\int \frac{Z(\nu) d\nu}{M\nu^2} \right)^{-1}, \quad (1)$$

where a is the bcc lattice parameter, α is a structure-dependent constant ($\alpha=0.0130$ for bcc structure), and M is the atomic mass. This ansatz starts from the idea that low-energy phonons contain information on the diffusion mechanism: they determine the directions along which the interatomic restoring forces are low. The model assumes that the diffusion jump—i.e., the most anharmonic motion imaginable—occurs in the direction of the weakest harmonic restoring forces. In the bcc alkali metals, a low migration energy has been shown to be associated with a low value of the shear modulus C' and a low-lying acoustic branch in the $\langle 110 \rangle$ direction. Strictly speaking, this formula is valid for monoatomic structure only, but Randl *et al.* have argued that this is a reasonable first approximation for DO_3 alloys, because the acoustic low-frequency modes giving the largest contribution to H_M involve mostly displacements of the heavy metal atoms.³⁵ A generalization of the model to binary intermetallics has been proposed by Kentzinger and Schober⁷² for $L1_2$ -ordered compounds; we will return to the most important points later. The Schober model is based on earlier ideas by Flynn⁷¹ who related the migration barrier to the elastic constants,

$$H_M^{elast} = \delta^2 C \Omega_0, \quad (2)$$

where C is an average elastic constant for migration given by

$$\frac{15}{2C} = \frac{3}{C_{11}} + \frac{1}{C'} + \frac{1}{C_{44}}. \quad (3)$$

Here δ is a dimensionless constant measuring the cutoff at which the harmonic potential is evaluated, $\delta^2=0.067$ for all bcc metals.⁷¹ Following these expressions and taking for M the average mass of the four atoms of the Fe_3Si cell, we find from the calculated phonon density of states an estimated migration energy of $H_M^{phon}=0.50$ eV which is very close to that derived by Randl *et al.* from a Born–von Karman fit of their inelastic neutron scattering experiments at 20 °C, $H_M^{phon}=0.59$ eV. Via the elastic constant approach, we calculated even slightly higher migration energies of $H_M^{elast}=0.73$ eV using the elastic constants measured by Kötter *et al.* and an even higher value of $H_M^{elast}=1.08$ eV using the set of elastic constants derived from the *ab initio*-calculated phonons. The migration enthalpies derived from the elastic constant are consistently larger than those deduced from the phonon spectra because this approach neglects the dispersion of the harmonic modes. Not unexpectedly, the migration energies calculated for Fe_3Si are of the same magnitude as those calculated for bcc Fe (for which Flynn reports a value

of $H_M^{elast}=0.70$ eV). Kentzinger *et al.*³⁷ and Randl *et al.*³⁶ have compared the migration enthalpies derived from the phonon spectra for pure Fe, $\text{Fe}_x\text{Al}_{1-x}$, and $\text{Fe}_x\text{Si}_{1-x}$. The conclusion was that the variation of H_M is far too small to explain the observed increase in the self-diffusion rate in the sequence Fe– Fe_3Al – Fe_3Si . Our results support the conclusion that the fast Fe diffusion in Fe_3Si cannot be attributed to the collective dynamics of the crystal lattice.

IV. ATOMIC DEFECTS

The formation of atomic defects in DO_3 Fe_3Si alloy close to the stoichiometry was studied within a mixed formalism^{46,73} combining *ab initio* theory and statistical mechanics. We consider in this study only single atomic vacancy and antistructure defects D on the various sublattices and do not take into account defect complexes. In the following, the notation V_ν stands for a vacancy on the ν sublattice ($\nu=\alpha, \beta$, or γ). Fe_β represents a Fe antistructure atom on the β sublattice, and Si_ν corresponds to a Si antistructure atom on the ν sublattice ($\nu=\alpha$ or γ). The theoretical formalism is first briefly described in Sec. IV A; then our results are presented in Sec. IV B.

A. Statistical mechanics: Grand canonical formalism

Since most experiments involve conservation of matter within the system under investigation, the defect formation parameters (energy E_D^f , volume Ω_D^f , and entropy S_D^f) related to a defect D are generally defined for constant particle number. For example, in monoatomic crystals the formation energy of a vacancy, E_V^f , can be easily defined as the sum of (i) the energy cost $\Delta\epsilon_V$ to remove an atom from an inner site and bring it to infinite distance from the sample and (ii) the energy gained by adding an atom to the system, which is statistically equal to the cohesive energy ϵ_0 of the ideal system. Similarly, the vacancy formation volume can be determined as $\Omega_V^f = \Delta V_V + \Omega_0$, where ΔV_V is the volume change induced by the relaxation of the crystal lattice around the vacancy V and Ω_0 the atomic volume in the ideal crystal.

In binary compounds such as $\text{Fe}_x\text{Si}_{1-x}$ the situation is much more complicated since different types of defects of both atomic species have to be created simultaneously to ensure a constant composition and coexist at concentrations of the same order. Therefore, for binary systems it is not meaningful to deal with the formation parameters related to one given type of defect *only*, but instead one has to define a set of *effective* defect parameters (hereafter noted \tilde{E}_D , $\tilde{\Omega}_D$, \tilde{S}_D) depending on the concentration and of the formation energy, volume and entropy parameters $\Delta\epsilon_D$, ΔV_D , and s_D of all involved defects D.

For systems with small defect concentrations c_D , Fähnle and co-workers^{46,73} have developed a grand-canonical formalism for the calculation of the effective defect formation parameters, in particular close to the stoichiometric composition. This approach is based on the minimization of the grand-canonical potential with respect to the defect concentrations c_D , while the conservation of particle numbers is

ensured through the introduction of chemical potentials μ_{Fe} and μ_{Si} .

As a result of the minimization of the grand potential, complex expressions for c_{D} as functions of temperature T , pressure p , and alloy composition x are obtained. However, if the T and p dependences of the chemical potentials, $\mu_{\text{Fe}}(T, p, x)$ and $\mu_{\text{Si}}(T, p, x)$, can be linearized, writing, for instance, $\mu_{\text{Fe}}(T, p, x) = \mu_{\text{Fe}}^0(x) + T\mu_{\text{Fe}}^T(x) + p\mu_{\text{Fe}}^p(x)$ (a situation which is generally the case under experimental conditions—i.e., at low T and p), one finds that the defect concentrations c_{D} can be approximated to high accuracy by

$$c_{\text{D}} \propto e^{\tilde{S}_{\text{D}} - (\tilde{E}_{\text{D}} + p\tilde{\Omega}_{\text{D}})/k_{\text{B}}T}, \quad (4)$$

where the effective defect formation parameters \tilde{E}_{D} and $\tilde{\Omega}_{\text{D}}$ are given by

$$\begin{aligned} \tilde{E}_{\text{V}_{\alpha}} &= \Delta\epsilon_{\text{V}_{\alpha}} + \mu_{\text{Fe}}^0, \\ \tilde{E}_{\text{V}_{\gamma}} &= \Delta\epsilon_{\text{V}_{\gamma}} + \mu_{\text{Fe}}^0, \\ \tilde{E}_{\text{V}_{\beta}} &= \Delta\epsilon_{\text{V}_{\beta}} + \mu_{\text{Si}}^0, \\ \tilde{E}_{\text{Si}_{\alpha}} &= \Delta\epsilon_{\text{Si}_{\alpha}} + \mu_{\text{Fe}}^0 - \mu_{\text{Si}}^0, \\ \tilde{E}_{\text{Si}_{\gamma}} &= \Delta\epsilon_{\text{Si}_{\gamma}} + \mu_{\text{Fe}}^0 - \mu_{\text{Si}}^0, \\ \tilde{E}_{\text{Fe}_{\beta}} &= \Delta\epsilon_{\text{Fe}_{\beta}} + \mu_{\text{Si}}^0 - \mu_{\text{Fe}}^0, \\ \tilde{\Omega}_{\text{V}_{\alpha}} &= \Delta V_{\text{V}_{\alpha}} + \mu_{\text{Fe}}^p, \\ \tilde{\Omega}_{\text{V}_{\gamma}} &= \Delta V_{\text{V}_{\gamma}} + \mu_{\text{Fe}}^p, \\ \tilde{\Omega}_{\text{V}_{\beta}} &= \Delta V_{\text{V}_{\beta}} + \mu_{\text{Si}}^p, \\ \tilde{\Omega}_{\text{Si}_{\alpha}} &= \Delta V_{\text{Si}_{\alpha}} + \mu_{\text{Fe}}^p - \mu_{\text{Si}}^p, \\ \tilde{\Omega}_{\text{Si}_{\gamma}} &= \Delta V_{\text{Si}_{\gamma}} + \mu_{\text{Fe}}^p - \mu_{\text{Si}}^p, \\ \tilde{\Omega}_{\text{Fe}_{\beta}} &= \Delta V_{\text{Fe}_{\beta}} + \mu_{\text{Si}}^p - \mu_{\text{Fe}}^p. \end{aligned} \quad (5)$$

Similar relations hold for the defect formation entropy \tilde{S}_{D} . However, in the cases considered below where an analytical resolution is possible, the equations to be solved are linear in the chemical potentials and in the defect formation parameters $\Delta\epsilon_{\text{D}}$, ΔV_{D} , and s_{D} . Therefore, the effective formation energies, volumes, and entropies \tilde{E}_{D} , $\tilde{\Omega}_{\text{D}}$, and \tilde{S}_{D} contain only the defect energy, volume, and entropy parameters, respectively. As a consequence, in this study we will neglect all entropy effects (otherwise very costly to calculate in an *ab initio* framework) since they affect only the prefactor of the concentrations c_{D} and, in the general case, only to a very limited extent the effective formation energies and

volumes.⁷⁴ Note that of course *absolute* values of c_{D} cannot be determined when using this approximation.

The energy and volume formation parameters $\Delta\epsilon_{\text{D}}$ and ΔV_{D} are assumed to be temperature and pressure independent. They are calculated at $T=0$ and $p=0$ within our *ab initio* framework as the changes in the total energy and volume of a large supercell, induced by removing an atom from the system (in the case of a vacancy) or by substituting an atom in its own sublattice by an atom of the other species (in the case of an antistructure defect). Note that the atoms are completely removed from the system and are not subsequently inserted at any lattice site. The $\Delta\epsilon_{\text{D}}$ thus represent grand-canonical defect excitation energies.

The contributions coming from the chemical potentials μ_{Fe} and μ_{Si} entering the expressions of \tilde{E}_{D} and $\tilde{\Omega}_{\text{D}}$ in Eqs. (5) are determined by two remaining conditions: the first one is the Gibbs-Duhem equation which at low defect concentrations simply states that

$$4(\epsilon_0 + p\Omega_0 - Ts_0) = 3\mu_{\text{Fe}}(T, p, x) + \mu_{\text{Si}}(T, p, x), \quad (6)$$

where ϵ_0 , Ω_0 , and s_0 are respectively defined as the cohesive energy per atom, the atomic volume, and the entropy per atom in the perfect crystal. In the limit $T=0$, $p=0$ this yields

$$\begin{aligned} 4\epsilon_0 &= 3\mu_{\text{Fe}}^0(x) + \mu_{\text{Si}}^0(x), \\ 4\Omega_0 &= 3\mu_{\text{Fe}}^p(x) + \mu_{\text{Si}}^p(x). \end{aligned} \quad (7)$$

Further, one imposes the condition that the numbers of Fe and Si atoms are conserved—i.e., that the composition of the $\text{Fe}_x\text{Si}_{1-x}$ alloy remains unchanged:

$$\frac{x}{1-x} = \frac{x - c_{\text{V}_{\alpha}} - c_{\text{V}_{\gamma}} - c_{\text{Si}_{\alpha}} - c_{\text{Si}_{\gamma}} + c_{\text{Fe}_{\beta}}}{1 - x - c_{\text{V}_{\beta}} - c_{\text{Fe}_{\beta}} + c_{\text{Si}_{\alpha}} + c_{\text{Si}_{\gamma}}}. \quad (8)$$

The solution of this coupled set of equations can be performed either numerically for any (T, p, x) conditions or analytically by introducing some simplifying assumption—for instance, that some types of defects occur at much higher concentrations than others. For example, if one assumes that the dominant structural defects in the stoichiometric Fe_3Si alloy are (as we will confirm in the next section) the Fe-antistructure defect on the β sublattice and the Si-antistructure defect on the α sublattice, one can neglect in Eq. (8) the concentrations of the other defects and simply rewrite it as $c_{\text{Fe}_{\beta}} = c_{\text{Si}_{\alpha}}$. Using Eqs. (5) and (7) this leads to the following simple analytical expressions for the effective formation energies and volumes:

$$\begin{aligned} \tilde{E}_{\text{Si}_{\gamma}} &= \tilde{E}_{\text{Fe}_{\beta}} = 1/2(\Delta\epsilon_{\text{Si}_{\gamma}} + \Delta\epsilon_{\text{Fe}_{\beta}}), \\ \tilde{E}_{\text{Si}_{\alpha}} &= \Delta\epsilon_{\text{Si}_{\alpha}} + 1/2(\Delta\epsilon_{\text{Fe}_{\beta}} - \Delta\epsilon_{\text{Si}_{\gamma}}), \\ \tilde{E}_{\text{V}_{\alpha}} &= \epsilon_0 + \Delta\epsilon_{\text{V}_{\alpha}} + 1/8(\Delta\epsilon_{\text{Fe}_{\beta}} - \Delta\epsilon_{\text{Si}_{\gamma}}), \\ \tilde{E}_{\text{V}_{\gamma}} &= \epsilon_0 + \Delta\epsilon_{\text{V}_{\gamma}} + 1/8(\Delta\epsilon_{\text{Fe}_{\beta}} - \Delta\epsilon_{\text{Si}_{\gamma}}), \\ \tilde{E}_{\text{V}_{\beta}} &= \epsilon_0 + \Delta\epsilon_{\text{V}_{\beta}} + 3/8(\Delta\epsilon_{\text{Si}_{\gamma}} - \Delta\epsilon_{\text{Fe}_{\beta}}), \end{aligned}$$

$$\begin{aligned}
\tilde{\Omega}_{\text{Si}_\gamma} &= \tilde{\Omega}_{\text{Fe}_\beta} = 1/2(\Delta V_{\text{Si}_\gamma} + \Delta V_{\text{Fe}_\beta}), \\
\tilde{\Omega}_{\text{Si}_\alpha} &= \Delta V_{\text{Si}_\alpha} + 1/2(\Delta V_{\text{Fe}_\beta} - \Delta V_{\text{Si}_\gamma}), \\
\tilde{\Omega}_{\text{V}_\alpha} &= \Omega_0 + \Delta V_{\text{V}_\alpha} + 1/8(\Delta V_{\text{Fe}_\beta} - \Delta V_{\text{Si}_\gamma}), \\
\tilde{\Omega}_{\text{V}_\gamma} &= \Omega_0 + \Delta V_{\text{V}_\gamma} + 1/8(\Delta V_{\text{Fe}_\beta} - \Delta V_{\text{Si}_\gamma}), \\
\tilde{\Omega}_{\text{V}_\beta} &= \Omega_0 + \Delta V_{\text{V}_\beta} + 3/8(\Delta V_{\text{Si}_\gamma} - \Delta V_{\text{Fe}_\beta}). \quad (9)
\end{aligned}$$

Obviously these expressions show that in contrast to monoatomic systems, here the effective formation parameters depend on the properties of all possible defects. They allow one to understand the influence of the condition of a fixed composition and of the basic assumptions on the nature of the dominant defect species on the effective formation energies and volumes of the other defects. For instance, the condition $\tilde{E}_{\text{Si}_\gamma} = \tilde{E}_{\text{Fe}_\beta}$ states that Si_γ - and Fe_β -antistructure defects must be simultaneously generated in order to keep the composition constant. As a consequence, to calculate the effective formation energy of a Si_α -antistructure defect at fixed stoichiometry, one must add to $\Delta\epsilon_{\text{Si}_\alpha}$ half of the difference in the formation energies of Fe_β - and Si_γ -antistructure defects, because the formation of a Si_α -antisite atom requires either the simultaneous formation of a Fe_β -antistructure defect or the transformation of a Si_γ into a Si_α defect. The remaining relations in Eqs. (9) can be interpreted in the same way.

We have performed also a full numerical solution of the equations determining the effective defects formation parameters. The comparison of these results with those obtained from the analytic expressions shows excellent agreement up to the melting temperature.

Analytical expressions can also be derived for small deviations from stoichiometry if one assumes the existence of a dominant structural defect—i.e., a defect that exists also at low T —while the concentrations of all other, thermal, defects become negligible. For example, for $\text{Fe}_x\text{Si}_{1-x}$ with $x \leq 0.75$, one can assume (as confirmed by the results of our *ab initio* calculations described in the following section) that the dominant structural defect is the Si-antistructure defect on the γ sublattice, due to its low formation energy in the stoichiometric compound. Under this assumption Eq. (8) is significantly simplified since we neglect all defect concentrations but c_{Si_γ} . The same derivation as above then leads to the following effective formation energies and volumes:

$$\begin{aligned}
\tilde{E}_{\text{Si}_\gamma} &= 0, \\
\tilde{E}_{\text{Fe}_\beta} &= \Delta\epsilon_{\text{Fe}_\beta} + \Delta\epsilon_{\text{Si}_\gamma}, \\
\tilde{E}_{\text{Si}_\alpha} &= \Delta\epsilon_{\text{Si}_\alpha} - \Delta\epsilon_{\text{Si}_\gamma}, \\
\tilde{E}_{\text{V}_\alpha} &= \epsilon_0 + \Delta\epsilon_{\text{V}_\alpha} - 1/4\Delta\epsilon_{\text{Si}_\gamma},
\end{aligned}$$

$$\begin{aligned}
\tilde{E}_{\text{V}_\gamma} &= \epsilon_0 + \Delta\epsilon_{\text{V}_\gamma} - 1/4\Delta\epsilon_{\text{Si}_\gamma}, \\
\tilde{E}_{\text{V}_\beta} &= \epsilon_0 + \Delta\epsilon_{\text{V}_\beta} + 3/4\Delta\epsilon_{\text{Si}_\gamma}, \\
\tilde{\Omega}_{\text{Si}_\gamma} &= 0, \\
\tilde{\Omega}_{\text{Fe}_\beta} &= \Delta V_{\text{Fe}_\beta} + \Delta V_{\text{Si}_\gamma}, \\
\tilde{\Omega}_{\text{Si}_\alpha} &= \Delta V_{\text{Si}_\alpha} - \Delta V_{\text{Si}_\gamma}, \\
\tilde{\Omega}_{\text{V}_\alpha} &= \Omega_0 + \Delta V_{\text{V}_\alpha} - 1/4\Delta V_{\text{Si}_\gamma}, \\
\tilde{\Omega}_{\text{V}_\gamma} &= \Omega_0 + \Delta V_{\text{V}_\gamma} - 1/4\Delta V_{\text{Si}_\gamma}, \\
\tilde{\Omega}_{\text{V}_\beta} &= \Omega_0 + \Delta V_{\text{V}_\beta} + 3/4\Delta V_{\text{Si}_\gamma}. \quad (10)
\end{aligned}$$

Similar expressions can be obtained for slightly Fe-rich alloys with $x \geq 0.75$ using the same approach and the assumption that the dominant structural defect is now the Fe-antistructure defect on the β sublattice, as we show below.

B. Effective defect formation energies and volumes

To determine the defect formation energies and volumes $\Delta\epsilon_{\text{D}}$ and ΔV_{D} , we have performed calculations on large 128-atom and small 32-atom supercells, performing a simultaneous relaxation of the volume of the supercell and of the internal coordinates. These parameters determine the effective defect formation volumes and energies $\tilde{\Omega}_{\text{D}}$ and \tilde{E}_{D} at fixed compositions. The influence of the relaxation on the calculated effective defect formation energies in the stoichiometric compound is illustrated in Table II. The strongest effect comes from a relaxation of the internal coordinates at fixed cell volume. For all vacancy formation energies, coordinate relaxation results in a reduction by ~ 0.3 – 0.4 eV. A reduction by an even larger amount is predicted for the formation of a Si-antisite defect on the α sublattice, while for a Si-antisite defect on the γ sublattice, the effect of atomic relaxation around the defect is relatively modest. The defect formation energy is lowest for an Fe-antisite defect on the β sublattice and the Si-antisite defect on the γ sublattice. In this case, relaxation reduces the formation energy from 0.53 eV to 0.42 eV. In comparison, the effect of an additional relaxation of the supercell volume is rather modest; it never exceeds 0.04 eV. This demonstrates that our supercells are large enough so that the strain field has decayed at the supercell boundary.

For the ideal stoichiometric compound we have calculated the effective defect formation energies either under the assumption that Fe-antistructure defects on the β sublattice and Si-antistructure defects on the γ sublattice dominate (i.e., $\tilde{E}_{\text{Si}_\gamma} = \tilde{E}_{\text{Fe}_\beta} \ll \tilde{E}_{\text{D}}$ for all other types of defects) or by allowing all other defects to appear at concentrations determined by the equilibrium conditions. Up to the highest temperatures of

TABLE II. Influence of relaxation on the effective defect formation energies (in eV) in stoichiometric Fe₃Si for vacancies on the α , β , and γ sublattices, for the Fe-antistructure atom on the β sublattice and for Si-antistructure atoms on the α and γ sublattices, as calculated with 128-atom supercells.

Relaxation	None	Fixed volume	Full
Si vacancy on β	2.88	2.55	2.52
Si antistructure on α	2.36	1.89	1.90
Fe vacancy on γ	1.72	1.30	1.28
Fe vacancy on α	1.26	0.97	0.93
Si antistructure on γ	0.53	0.42	0.40
Fe antistructure on β	0.53	0.42	0.40

interest, both results are essentially indistinguishable. For the Fe-enriched alloy, the constraint is $\tilde{E}_{\text{Fe}\beta}=0$; for the Fe-deficient alloy, $\tilde{E}_{\text{Si}\gamma}=0$. The results for the effective defect formation energies are compiled in Table III; the results for the formation volumes are listed in Table IV. For all vacancies, on both the Fe and Si sublattices, the effective formation volume is nearly equal to the average volume per atom. Our result is in very good agreement with the experimental estimate of Broska *et al.*⁷⁵ who estimated a vacancy formation volume of $0.9\Omega_0$ from the Doppler broadening of the positron annihilation under pressure. However, our results differ significantly from the calculations of Fähnle and Schimmele⁴² who derived values of 0.8, 0.44, and 0.36 (in units of Ω_0) for vacancies on the α , β , and γ sublattices from their calculations on 32-atom supercells. We have repeated our calculations for the smaller 32-atom cells, deriving effective formation volumes of 0.69, 0.63, and 0.68 in the same units. This confirms that larger supercells are required to achieve accurate results for the vacancy formation volumes.

Significant differences also exist for the effective vacancy formation energies where our results for large supercells are about 0.2–0.25 eV smaller than the earlier results of Fähnle and Schimmele.⁴² Smaller differences of 0.05 eV exist for the formation energies of antistructure defects. To elucidate the reasons for these discrepancies we have repeated our cal-

culations for 32-atom supercells. While for antisite defects we note almost perfect agreement between both sets of 32-atom calculations, for vacancies our formation energies are consistently lower by about 0.1 eV. The calculations of Fähnle and Schimmele have been performed using the full-potential-linearized augmented-plane-wave (FLAPW) method and the same GGA functional and should, in principle, lead to complete agreement with the present PAW calculations. However, as no information on the computational setup (cutoff energies, \mathbf{k} -space grids, etc.) is given, the reasons for the subsisting small differences are very difficult to assess.

Comparison of the 128- and 32-atom calculations shows that the larger supercells lead to consistently lower defect formation energies. For the formation of Fe-antistructure defects on the β sublattice and Si-antistructure defects on the γ sublattice the energy is reduced from 0.48 eV to 0.40 eV. This leads to an even stronger dominance of antisite defects in the stoichiometric compound, justifying the basic assumption leading to the analytic solution of the statistical-mechanical equations. The effective formation energies for vacancies decrease with decreasing concentration of the species: $\tilde{E}_{\text{V}\alpha}$ and $\tilde{E}_{\text{V}\gamma}$ decrease with decreasing Fe content, while $\tilde{E}_{\text{V}\beta}$ increases in the Fe-deficient alloy. For stoichiometric Fe₃Si Kümmerle *et al.*¹⁷ and Kerl *et al.*⁴⁰ found effective

TABLE III. Defect formation energies $\Delta\epsilon_D$ from the *ab initio* DFT calculations and effective defect formation energies \tilde{E}_D derived using the grand-canonical approach (all in eV) in Fe_xSi_{1-x} for vacancies on the α , β , and γ sublattices, for the Fe-antistructure atom on the β sublattice and for Si-antistructure atoms on the α and γ sublattices. Relaxation around the defects is fully taken into account. Results are given for 128- and 32-atom supercells (see text) with $\epsilon_0=-7.91$ eV. For the sake of comparison, previous results from Fähnle *et al.* obtained with a 32-atom supercell (Ref. 42) are also presented (in italics).

Fe concentration x_{Fe}	$x_{\text{Fe}} < 0.75$					$x_{\text{Fe}} = 0.75$			$x_{\text{Fe}} > 0.75$		
	$\Delta\epsilon_D$		\tilde{E}_D with $\tilde{E}_{\text{Si}\gamma}=0$		Ref. 42	\tilde{E}_D with $\tilde{E}_{\text{Si}\gamma}=\tilde{E}_{\text{Fe}\beta}$		\tilde{E}_D with $\tilde{E}_{\text{Fe}\beta}=0$			
	128 at.	32 at.	128 at.	32 at.		128 at.	32 at.	Ref. 42	128 at.	32 at.	Ref. 42
Si vacancy on β	9.05	9.13	2.82	3.04		2.52	2.68		2.22	2.32	
Si antistructure on α	3.74	3.95	1.51	1.52		1.90	1.99		2.30	2.47	
Fe vacancy on γ	9.65	9.82	1.18	1.30	<i>1.41</i>	1.28	1.42	<i>1.52</i>	1.38	1.54	<i>1.68</i>
Fe vacancy on α	9.30	9.47	0.83	0.95	<i>1.03</i>	0.93	1.07	<i>1.14</i>	1.03	1.19	<i>1.25</i>
Si antistructure on γ	2.24	2.43	0.00	0.00	<i>0.00</i>	0.40	0.48	<i>0.45</i>	0.80	0.95	<i>0.90</i>
Fe antistructure on β	-1.44	-1.48	0.80	0.95	<i>0.90</i>	0.40	0.48	<i>0.45</i>	0.00	0.00	<i>0.00</i>

vacancy formation energies of 1.05 eV and 0.74 eV from positron annihilation Doppler broadening and lifetime experiments. For slightly Fe-enriched samples formation energies ranging between 0.96 eV and 1.22 eV were derived from absolute vacancy concentrations determined from simultaneous measurements of the relative changes of the macroscopic dimensions of the sample and of the lattice parameters⁴⁰ and from positron annihilation.¹⁷ Both the absolute values and the concentration dependence are in good agreement with our results. The formation energy for Si vacancies on the β sublattice can only be estimated from tracer-diffusion experiments on Ge serving as a substitute for Si. Gude and Mehrer²⁴ report very large activation energies of 3.25–3.6 eV for slightly Fe-enriched samples. Assuming that the vacancy formation energy makes a major contribution to the activation energy, this is in very good agreement with our results.

Our calculations confirm that in Fe_3Si vacancies are formed predominantly on the Fe sublattices, with a somewhat lower vacancy concentration on the γ than on the α sublattice. However, the differences in the formation energies are not large enough to exclude the presence of thermal vacancies on both metallic sublattices. The formation energies for antisite defects are substantially lower than the vacancy formation energies (with the exception of a Si antistructure atom on the α sublattice). In stoichiometric Fe_3Si , the energy of formation for a Si antistructure atom is 0.4 eV on the γ site; the same energy is required for the formation of an Fe_β -antistructure atom. However, this result must be considered in conjunction with the very high formation energy of a vacancy on the β sublattice.

With increasing Fe content the effective formation energies for vacancies on the α and γ sublattices increase, accompanied by an increase of the effective formation energies for Si-antistructure defects on γ sites. The formation energies for Si vacancies and Si_α -antisite defects decrease, but remain much higher than the formation energies for Fe vacancies. For pure α -Fe, Domain and Becquart⁷⁶ calculated (also using VASP) an effective vacancy formation energy of 1.95 eV, to compare with experimental values of 2.0 eV,⁷⁷ 1.9 eV,⁷⁸ and 1.53 eV.⁷⁹ Domain and Becquart derived an effective vacancy formation volume of $0.90\Omega_0$, in good agreement with an experimental value⁸⁰ of $0.95\Omega_0$.

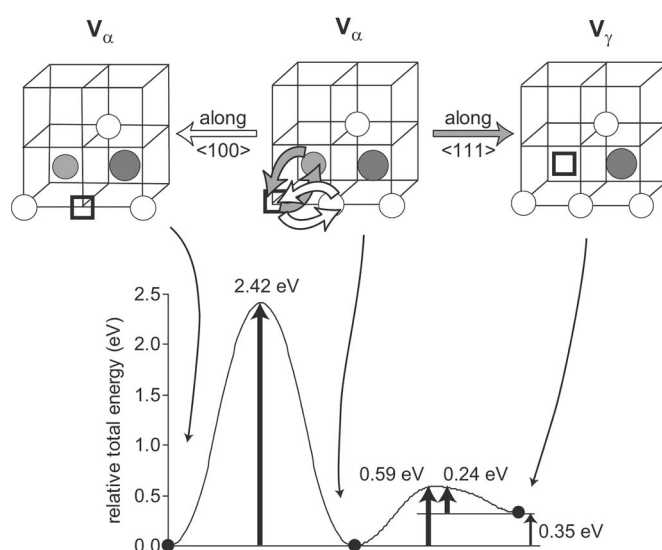


FIG. 3. Diffusion of a Fe vacancy on the α sublattice in the ideal stoichiometric alloy, along the two possible $\langle 100 \rangle$ (left) and $\langle 111 \rangle$ (right) directions.

V. DIFFUSION

To develop an atomistic scenario for diffusion, it is necessary to determine the activation energies for the most important hopping processes. We first present the results of our nudged-elastic-band calculations for the migration of isolated vacancies in the stoichiometric compound. Both in the stoichiometric and in the slightly Fe- or Si-enriched compounds, antisite atoms are the dominant defect species. Hence we must in addition consider vacancy diffusion processes in the vicinity of antistructure defects.

A. Migration of isolated vacancies

Figure 3 shows a schematic energy profile for the diffusion of a vacancy initially located on the α sublattice along the $\langle 100 \rangle$ direction into a next-nearest-neighbor position or along the $\langle 111 \rangle$ direction into a nearest-neighbor site. The activation energies are the saddle-point energies determined using the NEB method with a full structural relaxation of the environment of the diffusing atom. For diffusion of the va-

TABLE IV. Defect formation volumes ΔV_D from the *ab initio* DFT calculations and effective defect formation volumes $\tilde{\Omega}_D$ derived using the grand-canonical approach for $\text{Fe}_x\text{Si}_{1-x}$ (in units of the atomic volume $\Omega_0=11.00 \text{ \AA}^3$ in the perfect crystal).

Fe concentration x_{Fe}	$x_{\text{Fe}} < 0.75$					$x_{\text{Fe}} = 0.75$			$x_{\text{Fe}} > 0.75$		
	ΔV_D		$\tilde{\Omega}_D$ with $\tilde{\Omega}_{\text{Si}_\gamma} = 0$			$\tilde{\Omega}_D$ with $\tilde{\Omega}_{\text{Si}_\gamma} = \tilde{\Omega}_{\text{Fe}_\beta}$			$\tilde{\Omega}_D$ with $\tilde{\Omega}_{\text{Fe}_\beta} = 0$		
	128 at.	32 at.	128 at.	32 at.	Ref. 42	128 at.	32 at.	Ref. 42	128 at.	32 at.	Ref. 42
Si vacancy on β	0.15	-0.16	1.04	0.67	0.36	0.88	0.63	0.36	0.72	0.58	0.36
Si antistructure on α	0.22	0.03	0.36	0.25		0.58	0.31		0.79	0.37	
Fe vacancy on γ	-0.08	-0.39	0.95	0.67	0.44	1.01	0.68	0.44	1.06	0.70	0.44
Fe vacancy on α	-0.10	-0.38	0.93	0.68	0.8	0.99	0.69	0.8	1.04	0.71	0.8
Si antistructure on γ	-0.14	-0.22	0.00	0.00		0.22	0.06		0.43	0.12	
Fe antistructure on β	0.57	0.34	0.43	0.12		0.22	0.06		0.00	0.00	

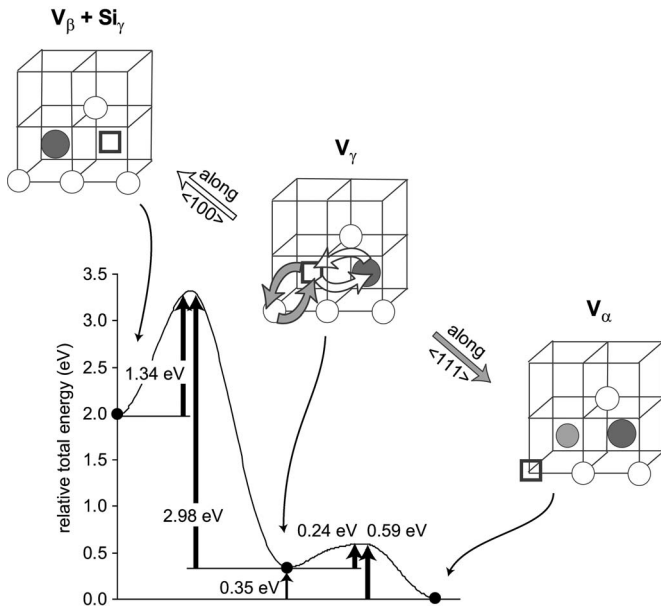


FIG. 4. Diffusion of a Fe vacancy on the γ sublattice in the ideal stoichiometric alloy, along the two possible $\langle 100 \rangle$ (left) and $\langle 111 \rangle$ (right) directions.

cancy along the $\langle 111 \rangle$ direction the final location of the vacancy is on the γ sublattice; i.e., this process is endothermic with a heat of reaction of 0.35 eV, equal to the difference in the effective vacancy formation energies on the two sublattices (see Table III). The activation energy for this process is 0.59 eV; for the inverse process it is only 0.24 eV. If the vacancy jumps along the $\langle 100 \rangle$ direction, it remains on the α sublattice. However, our calculations show that this process is suppressed by a very high activation barrier of 2.42 eV.

If the vacancy is initially located on the γ sublattice, a jump along the $\langle 111 \rangle$ direction corresponds (see Fig. 4) just to the inverse of the process described above; the process is exothermic with an energy gain of 0.35 eV and has a very low activation energy of 0.24 eV. If the vacancy moves along the $\langle 100 \rangle$ direction, a Si vacancy on the β sublattice and a Si-antisite defect on the γ sublattice are created. This process is strongly endothermic, with a heat of reaction of formation of 1.64 eV, equal to the difference in the effective

formation energies of the isolated defects, $\tilde{E}_{V_\beta} + \tilde{E}_{Si_\gamma} - \tilde{E}_{V_\gamma} = 1.64$ eV. This means that the interaction between vacancy and antistructure defect is negligible even at these short distances. Even more important is the very high activation energy of 2.98 eV for this process. The conclusion is that diffusion can occur only by nearest-neighbor jumps along the $\langle 111 \rangle$ direction; next-nearest neighbor jumps along the $\langle 100 \rangle$ directions are forbidden because of very high activation energies (although the jump distances differ only by 15%).

Figure 5 shows the energy profile for a sequence of vacancy jumps along $\langle 111 \rangle$. The activation energy for the first move from the α to the γ sublattice has an activation energy of 0.59 eV; the second move to a crystallographically equivalent α site is exothermic and has an even lower barrier of only 0.24 eV. But the next vacancy jump along the same direction would lead to the formation of a Si vacancy on the β sublattice and a Si-antistructure defect on the α sublattice. From the effective formation energies of the isolated defects we estimate a heat of reaction of $\tilde{E}_{V_\beta} + \tilde{E}_{Si_\alpha} - \tilde{E}_{V_\alpha} = 3.49$ eV. Optimization of the structure of the vacancy-antistructure defect pair leads to a slightly lower energy of 3.34 eV (see Fig. 5). However, we find this defect complex to be highly unstable; there is no energy barrier preventing the Si atom from jumping back to the β site.

Hence we find that in stoichiometric Fe_3Si diffusion proceeds by the migration of vacancies on the Fe sublattices, the formation of vacancies being disfavored by a very large vacancy formation energy. The dominant diffusion mechanism is a nearest-neighbor jump along the $\langle 111 \rangle$ directions, with very low migration energies: 0.24 eV for the jump of a vacancy from a γ to an α site and 0.59 eV for a migration in the opposite direction. Jumps along the $\langle 100 \rangle$ directions are prohibited because they require very high activation energies. Jump processes leading to the formation of Si-antistructure defects are blocked, because the simultaneous formation of a vacancy on the Si sublattice leads to an unstable situation which requires a high activation energy.

Comparison of the vacancy migration energies derived from the saddle-point energies with estimates based on the phonon spectrum is complicated by the fact that the energies of the lattice before and after the vacancy jump differ by a bias $\Delta = \tilde{E}_{V_\gamma} - \tilde{E}_{V_\alpha} = 0.35$ eV. The generalization of the

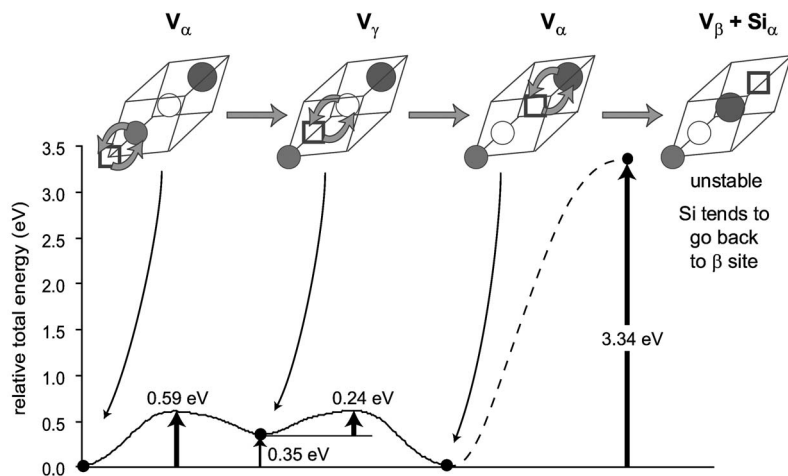


FIG. 5. Diffusion of a vacancy along the $\langle 111 \rangle$ direction in the ideal stoichiometric alloy. The dashed line indicates the pseudobarrier (3.34 eV) defined as the energy difference between the relaxed structure with an α vacancy and the nonrelaxed one with a β vacancy.

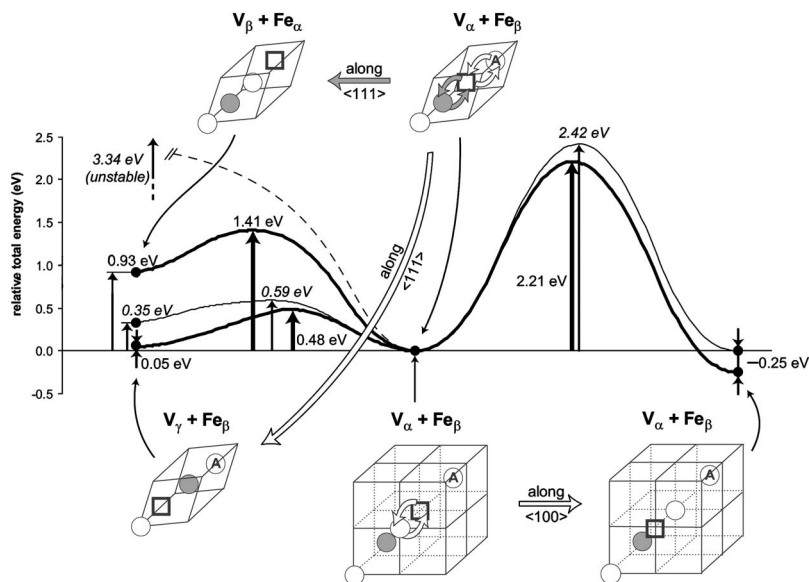


FIG. 6. Diffusion of a Fe vacancy on the α sublattice in vicinity to an Fe-antistructure atom on the β sublattice (indicated by a letter A), along the two possible $\langle 100 \rangle$ and $\langle 111 \rangle$ directions. Thin solid lines and values in italics correspond to the barriers calculated for the ideal stoichiometric alloy (cf. Fig. 3).

Schober model to a binary intermetallic compound and to jumps involving a change of the sublattice has been discussed by Kentzinger and Schober⁷² for $L1_2$ -type compounds. The present case is even simpler, because the jump does not lead to the formation of an antistructure defect. Furthermore, the path of minimal energy is straight by symmetry; the bias Δ is caused only by the different chemical environment of an Fe atom on α and γ sites. In this the migration energy derived from the phonon approach (neglecting the difference in the partial phonon DOS of Fe atoms on both sublattices) yields not the migration enthalpy H_M , but an activation energy $E_a = H_M - \frac{\Delta}{2}$ measured relative to the average energy of the lattice with a vacancy on an α and on a γ site, which is the same for jumps in both directions. In our case, $E_a = 0.415$ eV. This activation energy is distinctly lower than the estimate from the phonon spectrum or on the elastic properties. A low migration energy for nearest-neighbor jumps along $\langle 111 \rangle$ would require, if phonon-assisted, a soft acoustic mode in that direction which does not exist in Fe_3Si .

Our value for the migration energy can be compared with the value of $H_M = 0.65$ eV for vacancy migration along $\langle 111 \rangle$ in α -Fe from the *ab initio* calculations of Domain and Beccart.⁷⁶ In this case the barrier derived from supercell (54-atom) calculations is in surprisingly good agreement with the estimates derived from the elastic constants of the phonon spectrum. Previous *ab initio* calculations of migration energies are very scarce. The comparison shows that the faster diffusion of Fe in Fe_3Si than in α -Fe is primarily due to a reduction of the vacancy formation energy and further to a lower vacancy migration energy.

B. Vacancy migration in the vicinity of an Fe-antistructure defect

Figure 6 shows the potential-energy profile for the migration of a vacancy initially located on the α sublattice in the presence of an Fe_β -antistructure defect. Vacancy jumps on the α sublattice, along the $\langle 100 \rangle$ direction, lead to a slight reduction of the total energy (via a reduction of the repulsive

defect interactions), but they are prohibited by a high activation energy of 2.2 eV (which is only slightly lower than for the same process in the absence of the antistructure defect).

By jumps along the $\langle 111 \rangle$ direction, the vacancy can change sites either with the Fe-antisite atom (leading to the formation of a vacancy on the β sublattice while all sites on the metallic sublattices are now occupied) or with the neighboring Fe_γ atom (resulting in the formation of a vacancy of the γ sublattice). For the former process the energy change estimated from the effective defect formation energies is 1.19 eV; here, we find that due to the reduction of the repulsive defect interaction in the final state, the reaction energy for this process is reduced to 0.93 eV, with a substantial barrier of 1.41 eV. For the second process, without the interaction between the defects, the reaction energy would be just equal to the difference in the effective formation energies of Fe vacancies on the α and γ sublattices—i.e., 0.35 eV. Again, the reduction of the repulsive defect interaction energies reduces the endothermicity to 0.05 eV and also lowers the barrier for the $V_\alpha \rightarrow V_\gamma$ jump from 0.59 eV for an isolated vacancy to 0.48 eV. On the other hand, this also means that the barrier for the reverse process $V_\gamma \rightarrow V_\alpha$ is increased from 0.26 eV to 0.43 eV if the vacancy approaches an Fe-antistructure defect. Hence in the vicinity of an Fe-antisite defect the chemical bias for vacancy jumps between the α and γ sublattices disappears almost completely.

C. Vacancy migration in the vicinity of a Si-antisite defect

Figure 7 shows the potential-energy profile for the migration of a vacancy initially located on the α sublattice and with a Si_γ -antistructure defect in a nearest-neighbor position. The presence of the Si-antisite defect lowers the activation energy for vacancy migration on the α sublattice along the $\langle 100 \rangle$ direction, as long as the vacancy remains at a nearest-neighbor distance from the antisite defect. However, the activation energy for this process remains very high, 1.84 eV. Processes bringing the vacancy into larger distances from the antisite defect are hardly affected.

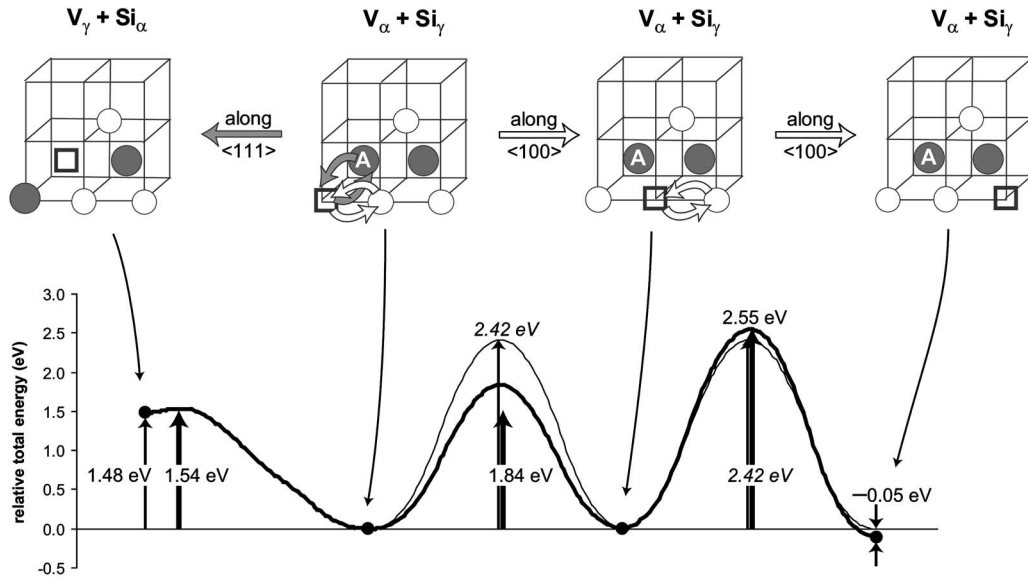


FIG. 7. Diffusion of a Fe vacancy on the α sublattice in vicinity to a Si-antistructure atom on the γ sublattice (indicated by a letter A), along the two possible $\langle 100 \rangle$ and $\langle 111 \rangle$ directions. Thin solid lines and values in italics correspond to the barriers calculated for the ideal stoichiometric alloy (cf. Fig. 3).

Migration along the $\langle 111 \rangle$ direction transforms the $V_\alpha + \text{Si}_\gamma$ defect pair into a $V_\gamma + \text{Si}_\alpha$ pair. From the effective formation energies of isolated vacancies, the reaction energy for this process is 1.86 eV. For the interacting defect complex, this energy is lowered to 1.48 eV. This process has a very late transition state with an activation energy of 1.54 eV. Altogether we find that the presence of a Si-antistructure defect very efficiently blocks the migration of vacancies in its immediate neighborhood.

VI. CONCLUSIONS AND OUTLOOK

We have presented a comprehensive investigation of defect formation and of single-particle and collective dynamics in the intermetallic compound Fe_3Si , using *ab initio* DFT and statistical mechanics in the grand-canonical ensemble. Our parameter-free calculations of the phonon dispersion relations achieve excellent agreement with the results of inelastic neutron scattering experiments, demonstrating the high accuracy of the interatomic forces derived from modern DFT calculations based on gradient-corrected exchange-correlation functionals. An important result is that our calculations confirm the absence of any anomalously soft phonon modes which could support a phonon-assisted mechanism for the fast self-diffusion in Fe_3Si .

For the calculation of the effective defect formation energies and volumes we have used total-energy calculations on large 128-atom supercells in combination with statistical mechanics in the grand-canonical ensemble, as described in the work of Fähnle and co-workers.^{42,46,73} In agreement with earlier results, we find that in the stoichiometric compound, the dominant defect species with the lowest effective formation energies of 0.4 eV are Fe-antisite atoms on the β sublattice and Si-antisite atoms on the γ sublattice. Vacancies on the metallic sublattices have effective formation energies of

0.93 eV (α sites) and 1.28 eV (γ sites), respectively. Effective formation energies for Si vacancies and Si-antistructure defects on the α sublattice are significantly higher. The formation energies derived from our calculations on large supercells are significantly lower than earlier results derived from smaller cells (we have checked the dependence on the model size to confirm that the reduction is really a size effect). Similarly, we have found that the use of a larger supercell leads to larger effective formation volumes. For both formation volumes and energies we find very good agreement with the available experimental data. The grand-canonical formalism allows us to estimate the change of the effective formation energies with composition—we find that the formation energies for Fe vacancies increase with increasing Fe content.

The nudged-elastic-band technique has been used to determine the activation energies for atomistic diffusion processes. We show that the diffusion of isolated vacancies proceeds by jumps between nearest-neighbor sites along the $\langle 111 \rangle$ direction. The migration of vacancies by next-nearest-neighbor jumps along the $\langle 100 \rangle$ direction is prohibited by high barriers. Vacancy diffusion occurs only on the metallic sublattices because of a prohibitively high energy for the formation of Si vacancies. We have also investigated the influence of the dominant structural defects: Fe_β - and Si_α -antistructure defects. The presence of a Fe_β -antistructure defect leads to a slight reduction of the barrier for vacancy diffusion on the metallic sublattices. The formation of a vacancy on the β sublattice by a site exchange between vacancies and antisite atoms is possible, but requires a high activation energy of 1.4 eV. In contrast, the presence of Si-antisite defects has a strong influence on vacancy diffusion, because the antisite atom very efficiently blocks diffusion on the metallic sublattice. This effect explains the decrease of the effective diffusion rate with increasing Si concentration.

The temperature dependence of self-diffusion is described by the expression

$$D = D_0 \exp\left(-\frac{Q}{k_B T}\right), \quad (11)$$

with the activation enthalpy Q determined by the sum of the vacancy formation energy \tilde{E}_V and the barrier for vacancy migration. Taking the average of our calculated effective vacancy formation energies of $\tilde{E}_{V_\alpha} = 0.93$ eV and $\tilde{E}_{V_\gamma} = 1.28$ eV and an average barrier for vacancy jumps along $\langle 111 \rangle$ of 0.42 eV we calculate an average activation energy for diffusion of $Q = 1.53$ eV. The experimental value of the activation enthalpy for self-diffusion in stoichiometric Fe₃Si determined by Mehrer *et al.*²⁷ using ⁵⁹Fe tracer experiments is $Q = 1.64$ eV, in good quantitative agreement with our results. Our predicted increase of the effective vacancy forma-

tion energies with increasing Fe content agrees with the increase of Q found in the tracer experiments. The result of a dominant diffusion mechanism by nearest-neighbor jumps along $\langle 111 \rangle$ agrees with the interpretation of the Mössbauer data.^{19,20,26} We conclude that advanced DFT calculations lead to a quantitatively accurate description of collective and single-particle dynamics in Fe₃Si.

ACKNOWLEDGMENTS

This work has been supported by the EU Commission within the STREP Project “Dynamics in Nano-Scale Materials” (Project No. NMP4-CT-2003-001516). The calculations were performed on Schrödinger II computer system at the Computer Center of Vienna University. We thank M. Jahnátek for the calculation of the elastic constants using the stress-strain relation. Stimulating discussions with G. Vogl and B. Sepiol are gratefully acknowledged.

*Present address: Laboratoire des Colloïdes, Verres et Nanomatériaux, Université de Montpellier II, 34095 Montpellier, France. Electronic address: dennler@lcvn.univ-montp2.fr

¹S. P. Murarka and M. C. Peckerar, in *Electronic Materials, Science and Technology*, edited by J. Streichen (Academic, Boston, 1989), p. 267.

²J. H. Westbrook and R. L. Fleischer, *Intermetallic Compounds—Principles and Practice* (Wiley, Chichester, 1994).

³G. Sauthoff, *Intermetallics* (VCH Verlag, Weinheim, 1995).

⁴J. E. Mattson, S. Kumar, E. E. Fullerton, S. R. Lee, C. H. Sowers, M. Grimsditch, S. D. Bader, and F. T. Parker, *Phys. Rev. Lett.* **71**, 185 (1993).

⁵K. Inomata, K. Yusu, and Y. Saito, *Phys. Rev. Lett.* **74**, 1863 (1995).

⁶J. Herfort, H. P. Schönherr, A. Kawaharzuka, M. Ramsteiner, and K. H. Ploog, *J. Cryst. Growth* **278**, 666 (2005).

⁷A. Ionescu, C. A. F. Vaz, T. Tripiniotis, C. M. Gurtler, H. Garcia-Miquel, J. A. C. Bland, M. E. Vickers, R. M. Dalgliesh, S. Langridge, Y. Bugoslavsky, Y. Miyoshi, L. Cohen, and K. R. A. Ziebeck, *Phys. Rev. B* **71**, 094401 (2005).

⁸T. Yoshitake, D. Nakagauchi, T. Ogawa, M. Itakura, N. Kuwano, Y. Tomokiyo, T. Kajiwara, and K. Nagayama, *Appl. Phys. Lett.* **86**, 262505 (2005).

⁹T. B. Massalski, *Binary Alloy Phase Diagrams* (American Society for Metals, Metals Park, OH, 1986).

¹⁰O. Kubaschewski, *Iron Binary Phase Diagrams* (Springer, Berlin, 1982).

¹¹P. Villars and L. D. Calvert, *Pearson's Handbook of Crystallographic Data for Intermetallic Phases* (American Society for Metals, Materials Park, OH, 1985).

¹²J. Wolff, M. Franz, A. Broska, R. Kerl, M. Weinlagen, B. Khler, M. Brauer, F. Faupel, and Th. Hehenkamp, *Intermetallics* **7**, 289 (1999).

¹³U. Kettner, H. Rehfeld, C. Engelke, and H. Neuhauser, *Intermetallics* **7**, 405 (1999).

¹⁴Y. Zhang and D. G. Ivey, *J. Mater. Sci.* **33**, 3131 (1998).

¹⁵P. Lejcek, O. Schneeweis, and A. Frankiewicz, *Surf. Sci.* **566**,

826 (2004).

¹⁶B. Zuo and T. Sritharan, *Acta Mater.* **53**, 1233 (2004).

¹⁷E. A. Kümmerle, K. Badura, B. Sepiol, H. Mehrer, and H. E. Schaefer, *Phys. Rev. B* **52**, R6947 (1995).

¹⁸R. Würschum, P. Farber, R. Dittmar, P. Scharwaechter, W. Frank, and H. E. Schaefer, *Phys. Rev. Lett.* **79**, 4918 (1997).

¹⁹B. Sepiol and G. Vogl, *Phys. Rev. Lett.* **71**, 731 (1993).

²⁰G. Vogl and B. Sepiol, *Acta Metall. Mater.* **42**, 3175 (1994).

²¹B. Sepiol and G. Vogl, *Hyperfine Interact.* **95**, 149 (1995).

²²H. Mehrer, *Mater. Trans., JIM* **37**, 1259 (1996).

²³A. Gude, K. Freitag, B. Sepiol, G. Vogl, and H. Mehrer, *Phys. Status Solidi B* **197**, 299 (1997).

²⁴A. Gude and H. Mehrer, *Philos. Mag. A* **76**, 1 (1997).

²⁵B. Sepiol, A. Meyer, V. G. Kohn, R. Ruffer, H. Franz, and G. Vogl, *Defect Diffus. Forum* **143**, 1311 (1997).

²⁶A. Gude, B. Sepiol, G. Vogl, and H. Mehrer, *Defect Diffus. Forum* **143**, 351 (1997).

²⁷H. Mehrer, M. Eggersmann, A. Gude, M. Salamon, and B. Sepiol, *Mater. Sci. Eng., A* **240**, 889 (1997).

²⁸I. V. Belova and G. E. Murch, *J. Phys. Chem. Solids* **59**, 1 (1998).

²⁹B. Sepiol, A. Meyer, G. Vogl, H. Franz, and R. Ruffer, *Phys. Rev. B* **57**, 10433 (1998).

³⁰G. Vogl, *High Temp. Mater. Processes* (N.Y., NY, U.S.) **18**, 293 (1999).

³¹G. Vogl and M. Hartmann, *J. Phys.: Condens. Matter* **13**, 7763 (2001).

³²M. Wellen, P. Fielitz, G. Borchardt, S. Weber, S. Scherrer, H. Mehrer, and B. Sepiol, *Defect Diffus. Forum* **194**, 499 (2001).

³³H. Thiess, B. Sepiol, R. Ruffer, and G. Vogl, *Defect Diffus. Forum* **194-1**, 363 (2001).

³⁴W. Petry, A. Heiming, C. Herzig, and W. Trampenau, *Defect Diffus. Forum* **75**, 211 (1991).

³⁵O. G. Randl, G. Vogl, W. Petry, B. Hennion, B. Sepiol, and K. Nembach, *J. Phys.: Condens. Matter* **7**, 5983 (1995).

³⁶O. G. Randl, G. Vogl, and W. Petry, *Physica B* **219-220**, 499 (1996).

- ³⁷E. Kentzinger, V. Pierron-Bohnes, M. C. Cadeville, W. Petry, and B. Hennion, *J. Phys.: Condens. Matter* **8**, 5535 (1996); *Defect Diffus. Forum* **143**, 365 (1997).
- ³⁸O. G. Randl, W. Petry, G. Vogl, W. Bühner, and B. Hennion, *J. Phys.: Condens. Matter* **9**, 10283 (1996).
- ³⁹H. E. Schaefer and K. Badura-Gergen, *Defect Diffus. Forum* **143**, 193 (1997).
- ⁴⁰R. Kerl, J. Wolff, and Th. Hehenkamp, *Intermetallics* **7**, 301 (1999).
- ⁴¹H. R. Schober, W. Petry, and J. Trampenau, *J. Phys.: Condens. Matter* **4**, 9321 (1992).
- ⁴²M. Fähnle and L. Schimmele, *Z. Metallkd.* **95**, 864 (2004).
- ⁴³J. Mayer, B. Meyer, J. S. Oehrens, G. Bester, N. Börnsen, and M. Fähnle, *Intermetallics* **5**, 597 (1997).
- ⁴⁴G. Bester, B. Meyer, and M. Fähnle, *Phys. Rev. B* **57**, R11019 (1998).
- ⁴⁵M. Fähnle, J. Mayer, and B. Meyer, *Intermetallics* **7**, 315 (1999).
- ⁴⁶B. Meyer and M. Fähnle, *Phys. Rev. B* **59**, 6072 (1999).
- ⁴⁷Y. Jirásková, O. Schneeweis, M. Šob, and M. Novotny, *Acta Mater.* **45**, 2147 (1997).
- ⁴⁸G. Kresse and J. Hafner, *Phys. Rev. B* **47**, R558 (1993).
- ⁴⁹G. Kresse and J. Furthmüller, *Phys. Rev. B* **54**, 11 169 (1996); *Comput. Mater. Sci.* **6**, 15 (1996).
- ⁵⁰P. E. Blöchl, *Phys. Rev. B* **50**, 17 953 (1994).
- ⁵¹G. Kresse and D. Joubert, *Phys. Rev. B* **59**, 1758 (1999).
- ⁵²H. J. Monkhorst and J. D. Pack, *Phys. Rev. B* **13**, 5188 (1976).
- ⁵³S. H. Vosko, L. Wilk, and M. Nusair, *Can. J. Phys.* **58**, 1200 (1980).
- ⁵⁴E. G. Moroni, W. Wolf, J. Hafner, and R. Podloucky, *Phys. Rev. B* **59**, 12860 (1999).
- ⁵⁵J. P. Perdew, K. Burke, and M. Ernzerhof, *Phys. Rev. Lett.* **77**, 3865 (1996).
- ⁵⁶J. P. Perdew, J. A. Chevary, S. H. Vosko, K. A. Jackson, M. R. Pederson, D. J. Singh, and C. Fiolhais, *Phys. Rev. B* **46**, 6671 (1992).
- ⁵⁷V. A. Niculescu, T. J. Burch, and J. I. Budnick, *J. Magn. Magn. Mater.* **39**, 223 (1983).
- ⁵⁸N. I. Kulikov, D. Fristot, J. Hugel, and A. V. Postnikov, *Comput. Mater. Sci.* **17**, 106 (2000); *Phys. Rev. B* **66**, 014206 (2002).
- ⁵⁹J. Kudrnovsky, N. E. Christensen, and O. K. Andersen, *Phys. Rev. B* **43**, 5924 (1991).
- ⁶⁰W. H. Press, S. A. Teukolsky, W. T. Vetterling, and B. P. Flannery, *Numerical Recipes* (Cambridge University Press, New York, 2002).
- ⁶¹G. Mills, H. Jonsson, and G. K. Schenter, *Surf. Sci.* **324**, 305 (1995).
- ⁶²A. Ulitski and R. Elber, *J. Chem. Phys.* **92**, 1510 (1990).
- ⁶³G. Kresse, J. Furthmüller, and J. Hafner, *Europhys. Lett.* **32**, 729 (1995).
- ⁶⁴R. M. Martin, *Phys. Rev.* **186**, 871 (1969).
- ⁶⁵M. T. Dove, *Introduction to Lattice Dynamics* (Cambridge University Press, Cambridge, England, 1993).
- ⁶⁶Y. Le Page and P. Saxe, *Phys. Rev. B* **63**, 174103 (2001).
- ⁶⁷M. Jahnátek, M. Krajčí, and J. Hafner, *Phys. Rev. B* **71**, 024101 (2005).
- ⁶⁸G. Kötter, K. Nembach, F. Wallow, and E. Nembach, *Mater. Sci. Eng., A* **114**, 29 (1989).
- ⁶⁹J. B. Rausch and F. X. Kayser, *J. Appl. Phys.* **48**, 487 (1977).
- ⁷⁰H. G. Drickamer, R. W. Lynch, R. L. Clendenen, and E. A. Perez-Albuere, *Solid State Phys.* **19**, 1359 (1966).
- ⁷¹C. P. Flynn, *Phys. Rev.* **171**, 682 (1968); **179**, 920(E) (1969).
- ⁷²E. Kentzinger and H. R. Schober, *J. Phys.: Condens. Matter* **12**, 8145 (2000).
- ⁷³J. Mayer and M. Fähnle, *Acta Mater.* **45**, 2207 (1997).
- ⁷⁴M. Fähnle, G. Bester, and B. Meyer, *Scr. Mater.* **39**, 1071 (1998).
- ⁷⁵A. Broska, J. Wolff, M. Franz, and Th. Hehenkamp, *Intermetallics* **7**, 289 (1999).
- ⁷⁶C. Domain and C. S. Becquart, *Phys. Rev. B* **65**, 024103 (2001).
- ⁷⁷L. De Schepper, D. Segers, L. Dorikens-Vanpraet, M. Dorikens, G. Knuyt, L. M. Stals, and P. Moser, *Phys. Rev. B* **27**, 5257 (1983).
- ⁷⁸H. Schultz, in *Atomic Defects in Metals*, edited by H. Ullmaier, Landolt-Börnstein, New Series, Group III, Vol. 25 (Springer, Berlin 1991).
- ⁷⁹H. E. Schäfer, K. Maier, M. Weller, D. Herlach, A. Seeger, and J. Diehl, *Scr. Metall.* **11**, 803 (1977).
- ⁸⁰P. Erhart, K. H. Robrock, and H. R. Schober, in *Physics of Radiation Effects in Crystals*, edited by R. A. Johnson and A. N. Orlov (Elsevier, Amsterdam, 1986), p. 63.